# Solid-State Thermionic Power Generators: An Analytical Analysis in the Nonlinear Regime

M. Zebarjadi*

*Department of Electrical and Computer Engineering, University of Virginia, Charlottesville, Virginia 22904, USA*
*and Department of Materials and Science Engineering, University of Virginia, Charlottesville, Virginia 22904, USA*

(Received 26 January 2017; revised manuscript received 11 May 2017; published 11 July 2017)

Solid-state thermionic power generators are an alternative to thermoelectric modules. In this paper, we develop an analytical model to investigate the performance of these generators in the nonlinear regime. We identify dimensionless parameters determining their performance and provide measures to estimate an acceptable range of thermal and electrical resistances of thermionic generators. We find the relation between the optimum load resistance and the internal resistance and suggest guidelines for the design of thermionic power generators. Finally, we show that in the nonlinear regime, thermionic power generators can have efficiency values higher than the state-of-the-art thermoelectric modules.

DOI: 10.1103/PhysRevApplied.8.014008

## I. INTRODUCTION

Solid-state thermionic power generators can be viewed as a bridge between vacuum-state thermionic convertors and thermoelectric power generators. Like many other heat engines, these devices can work either as power generators where they convert input heat to electricity or coolers where applied electricity is used to pump heat. Solid-state thermionic coolers and power generators were proposed by Mahan *et al.* [1,2] and Shakouri *et al.* [3,4]. The working principles of solid-state thermionic convertors are very similar to vacuum-state thermionic convertors. In vacuum-state thermionic conversion, a cathode and an anode are separated by vacuum. Electrons in the cathode are heated to high energies. When they gain enough velocity in the out-of-plane direction to overcome the energy barrier (the cathode's work function), they leave the cathode and enter the vacuum. Some of these electrons are eventually collected at the anode side and flow through the outer circuit. Vacuum thermionic diodes were invented in 1904 and were used in radio and telephone communications. However, it was only in 1956 that two distinct practical versions of thermionic power generators were made by Wilson [5] and Hatsopoulos and Kaye [6]. Efficiencies as high as 16% and large power densities reaching 11 $\mathrm{W\,cm^{-2}}$ were reported in early demonstrations [7].

The main drawback of vacuum-state thermionic convertors is that they can operate only at high temperatures ($>$1000 K). In solid-state thermionic convertors, the vacuum is replaced by a solid, usually a semiconductor. Solid-state thermionic convertors have several advantages to vacuum-state thermionic convertors. First, the effective barrier height is the difference between the cathode's work function and the semiconductor's electron affinity. Therefore, it is easy to design solid-state thermionic devices with small barrier height and extend the operation temperature to low temperatures. Second, the absence of vacuum makes the fabrication process and access to the cathode and anode for the purpose of heating and cooling, easier. Finally, vacuum thermionic convertors suffer from the space-charge effect. This effect is negligible in solid-state thermionic convertors due to the extremely small size of the barrier region and the fact that the chemical potential of the semiconductors can be tuned by means of doping to minimize the band bending (which is the equivalent of the space-charge effect in vacuum-state devices). The main disadvantage of the solid-state thermionic convertors is their heat leakage by conduction through the semiconductor which is more severe compared to thermal radiation in vacuum-state thermionic convertors. This thermal leakage was noted from the very beginning by Mahan and Woods [2] who then proposed that only small temperature differences should be imposed to each barrier, and multibarrier structures should be used. Shakouri *et al.* [3] proposed that tall barriers in the electron path could be used to filter high-energy electrons and increase the average energy per carrier to increase the efficiency. In recent years, there has been some renewed interest in solid-state thermionic power generation using van der Waals heterostructures [8–10].

In this work, we develop an analytical model to investigate the operation limits of solid-state thermionic power generators. We focus on tall barriers and large temperature differences. The linear regime of small temperature differences has been investigated before by Vining and Mahan [11]. They showed that in the linear limit, thermoelectric convertors outperform thermionic convertors.

## II. MODEL

Consider a single-barrier structure. The cathode and anode are separated by a semiconductor. The semiconductor

*m.zebarjadi@virginia.edu

 

thickness is smaller than the electron mean free path, ensuring ballistic transport. We define an internal resistance for the structure $R$. Ideally this internal resistance should be zero. In practice, it is never zero, and even for a purely ballistic channel, it has the contribution of the cathode and anode resistances, the interfacial resistances, and even the outer circuit connecting wire resistances. Moss [12] investigated the importance of the internal resistance on the performance of the thermionic generators. In the context of vacuum-state thermionic generators, she concluded that even a small internal resistance (fraction of an ohm) drops the output power.

We also define a thermal resistance $R_t$, which includes the thermal resistance of the barrier layer and the interfacial resistance between the barrier, cathode, and anode layers. Ideally, this resistance should be infinitely large. Since the thickness of the barrier region is small, its thermal resistance is also small. Therefore, a good design requires large interfacial thermal resistances. Assuming the barrier is tall, the electron population above the barrier can be approximated by the Maxwellian distribution and the current can be described by the Richardson-Dushman current. In a typical vacuum thermionic convertor, the cathode's work function is larger than the anode's work function. There are two distinct operating regions: (1) when the cathode's work function $\phi_c$ is larger than the anode's work function $\phi_a$ plus the total voltage ($V = IR + IR_l$, $R_l$ is the load resistance) and (2) the opposite case when $\phi_c < \phi_a + V$.

It can be easily shown that in the first case, the current is independent of $\phi_a$, and in the second case. it is independent of $\phi_c$.

In case 1, the reverse current from the anode to the cathode is small, and the current is almost constant with respect to voltage, while in case 2, the current drops exponentially with respect to the voltage. We write our equations for case 1, and we assume that the optimum power with respect to current and voltage happens in this regime. The electrical and thermal current, power, and efficiency for ($\phi_c > \phi_a + V$) can be written as [1,12]

$$J = A_R T_c^2 \exp\left(-\frac{e\phi_c}{k_B T_c}\right) - A_R T_a^2 \exp\left(-\frac{e(\phi_c - V)}{k_B T_a}\right), \tag{1}$$

$$J_{Qc} = A_R T_c^2 \exp\left(-\frac{e\phi_c}{k_B T_c}\right)(\phi_c + 2k_B T_c/e) - A_R T_a^2 \exp\left(-\frac{e(\phi_c - V)}{k_B T_a}\right)(\phi_c + 2k_B T_a/e) + \frac{T_c - T_a}{R_t}, \tag{2}$$

$$p = \frac{P}{A} = IR_l J = (V - IR)J, \tag{3}$$

$$\eta = \frac{p}{J_{Qc}}. \tag{4}$$

$J$ is the electrical current density, $I$ is the electrical current, $J_{Qc}$ is the thermal current density at the cathode-barrier junction, $p$ is the power density dissipated in the load, $P$ is the power delivered to the load, $A$ is the cross section area, and $\eta$ is the efficiency of thermal to electrical energy conversion. $T_c$ is the cathode temperature (hot), $T_a$ is the anode temperature (cold), $k_B$ is the Boltzmann constant, $e$ is the electric charge, and $A_R$ is the Richardson constant containing effective masses of the cathode and anode and the average transmission function. To have zero current at zero voltage and zero temperature gradient, $A_R$ should be the same for both the cathode and anode current.

The first term in Eq. (1) is the current from the cathode to the anode, and the second term is that from the anode to the cathode. Similarly, in Eq. (2), the first term is the thermal current from the cathode to the anode, and the second term is the backflow from the anode to the cathode. The third term in Eq. (2) is the lattice conduction term or the heat leak via the barrier's lattice and from the cathode to the anode. Here we neglect Joule heating inside the barrier, as we assume ballistic transport. Note that there is Joule heating outside of the barrier in the cathode and the anode region, but that is not of interest. As long as the electron-phonon mean free path is larger than the barrier thickness, the Joule heating within the barrier can be ignored.

To make the analysis simple, we define the dimensionless parameters as listed below:

$$\Phi_c = \frac{e\phi_c}{k_B T_c}, \quad \Phi_a = \frac{e\phi_a}{k_B T_a}, \quad V_a = \frac{\mathrm{eV}}{k_B T_a}, \quad \theta = \frac{T_c}{T_a},$$
$$J_D = \frac{J}{A_R T_a^2}, \quad J_{QD} = \frac{eJ_Q}{k_B T_a A_R T_a^2}, \quad P_D = \frac{ep}{k_B T_a A_R T_a^2}. \tag{5}$$

We use subscript $D$ to refer to dimensionless current and power. Now we can rewrite Eqs. (1)–(4), in a dimensionless format:

$$J_D = \theta^2 \exp(-\Phi_c) - \exp(-\Phi_c\theta + V_a) = J_c - J_0 \exp(V_a), \tag{6}$$

$$J_a = J_0 \exp(V_a), \tag{7}$$

$$J_c = \theta^2 \exp(-\Phi_c), \tag{8}$$

$$J_0 = \exp(-\Phi_c\theta), \tag{9}$$

$$V_a = \ln\left(\frac{J_c - J_D}{J_0}\right), \tag{10}$$

$$J_{QD} = J_c(\Phi_c\theta + 2\theta) - J_0 \exp(V_a)(\Phi_c\theta + 2) + \frac{\theta - 1}{R_{tD}}, \tag{11}$$

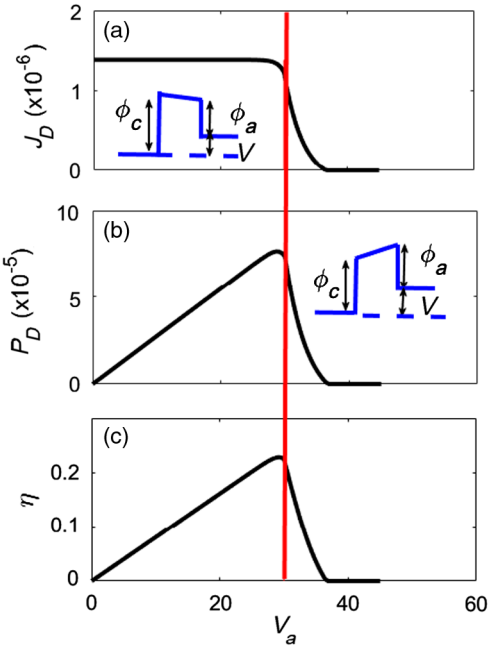


FIG. 1. Dimensionless current, power, and efficiency versus voltage for $\theta = 3$, $R_D = R_{tD} = 10000$, $\Phi_c = 15$, and $\Phi_a = 15$. The red line ($V_a = \Phi_c\theta - \Phi_a$) is separating the two operating regions discussed in the text. A schematic of the band diagram in case 1 is shown as an inset of plot (a) and a schematic of the band diagram in case 2 is shown as an inset of plot (b).

$$R_{tD} = R_t k_B A_R T_a^2/e, \tag{12}$$

$$P_D = (V_a - J_D R_D)J_D, \tag{13}$$

$$R_D = \frac{A_R T_a A R e}{k_B}. \tag{14}$$

$R_{tD}$ is the dimensionless internal thermal resistance, and the $R_D$ is the dimensionless internal electrical resistance.

Similar equations can be written for the second case where $\phi_c < \phi_a + V$.

These equations can be solved numerically. However, it is the purpose of this work to find analytical solutions. Before we move on to analytical solutions, let us first look at the numerical results to develop an understanding of the performance of the device. Figure 1 shows the numerical results for a given set of parameters. The values of the parameters used are shown in the caption of Fig. 1.

## III. RESULTS

Now let us discuss the optimum performance of the device analytically. We note that the optimum power and the optimum efficiency do not happen at exactly the same current or voltage but at very close ones. We first optimize the power with respect to the current. Taking the derivative of Eq. (13) with respect to the current and setting it to zero, we find the optimal condition to be

$$\left(\frac{1}{J_c - J_D} + 2R_D\right)J_D = V_a = J_D(R_D + R_{lD}). \tag{15}$$

Therefore, when power is maximum, the following relation holds between the load resistance and the internal resistance:

$$\frac{1}{J_a} + R_D = R_{lD}. \tag{16}$$

To find the optimum current we use Eqs. (15) and (10) and we find

$$J_c + (2J_c R_D - 1)J_a - 2R_D J_a^2 = J_a \ln\left(\frac{J_a}{J_0}\right). \tag{17}$$

This equation does not have an analytical solution. However, the second-order term in $J_a$ is small and can be neglected. We then find at the optimum power:

$$J_a \approx \frac{J_c}{LW(x_0)}, \tag{18}$$

$$x_0 = \theta^2 \exp[(\theta - 1)\Phi_c + 1 - 2J_c R_D]. \tag{19}$$

Here, $LW$ is the Lambert $W$ function (see the Appendix).

Finally, the optimum current, corresponding load resistance, optimum power, and corresponding efficiency can be written as

$$J_D = J_c y, \tag{20}$$

$$y = 1 - \frac{1}{LW(x_0)}, \tag{21}$$

$$\frac{LW(x_0)}{J_c} + R_D = R_l, \tag{22}$$

$$P_{D_{\text{opt}}} = [J_C R_D + LW(x_0)]J_c y^2, \tag{23}$$

$$\eta = \frac{[J_c R_D + LW(x_0)]y^2}{(\Phi_c\theta + 2)y + (2 + \frac{1}{J_c R_{tD}})(\theta - 1)}. \tag{24}$$

Two immediate conclusions can be drawn regarding the acceptable range of the internal resistances. For electrical resistance, noting that $(\theta - 1)\Phi_c > 0$, we find that if $2J_c R_D \ll 1$, then the effect of internal resistance is very small [Eq. (19)] and does not substantially drop the power. The criteria can be written as $R \ll 0.5(k_B T_a/eJ_R A)$, where $J_R$ is the Richardson current (in units of amperes) from the cathode to the anode. If we use the theoretical Richardson constant, $A_R$ of 120 A cm$^{-2}$ K$^{-2}$, barrier height $\Phi_c$ of 5, cathode and anode area $A$ of 1 cm$^2$, $T_a$ of 300 K, and $T_c = 400$ K, we find $R \ll 1 \times 10^{-7}$ $\Omega(R_D \sim 44)$, which means any internal resistance larger than $10^{-7}$ $\Omega$ lowers the

output power from that of an ideal thermionic convertor and cannot be neglected. The value of the maximum negligible $R$ can be increased by increasing the barrier height. Increasing $\Phi_c$ from 5 to 10 and 15, increases the $R$ limit to 15 $\mu\Omega$ and 2.2 m$\Omega$, respectively. The internal resistance includes resistances of the layers (barrier, cathode, and anode) and the interfacial resistances. The resistance of the barrier layer is much smaller since the thickness is small (less than 100 nm). The resistance of the cathode and anode can also be kept small. The resistance of a typical metal of thickness 1 mm and area of 1 cm$^2$ is $R \sim 10^{-8}\ \Omega\text{m} \times 10^{-3}\ \text{m}/10^{-4}\ \text{m}^2 = 10^{-7}\ \Omega$. Because of the low resistance of the barrier and electrodes, the interfacial resistance might play an important role. It is, therefore, crucial to keep the interfacial electrical resistance low, for example, by aligning the work function of the barrier and cathode to create a linear voltage drop over the barrier layer and, therefore, to prevent a Schottky barrier.

Similarly, for the thermal resistance, we can conclude that if $J_c R_{tD} \gg 1$, then the lattice thermal conduction is minimal and will not substantially drop the efficiency. This condition is equivalent to $R_t \gg (e/k_B J_R)$. Using the same parameters as before, we find $R_t \gg 9 \times 10^{-6}$ m$^2$ K W$^{-1}$ or $G_t \ll 0.1$ MW m$^{-2}$ K$^{-1}$, which is extremely small and is very challenging to obtain. If we take a typical material with thermal conductivity of 1 W m$^{-1}$ K$^{-1}$ and thickness of 100 nm, then the equivalent $G_t = (\kappa/L) = 10$ MW m$^{-2}$ K$^{-1}$. Of course, if we increase the thickness, we can lower the conductance to an arbitrarily low value. However, we note that the criterion for thermionic emission is that the thickness should be smaller than the electron mean free path. Therefore, it is not possible to lower the conductance without breaking the thermionic conditions. We believe one possible solution is to use weakly bonded materials such as layered van der Waals heterostructures. In a recent work [9], we show that for layered materials, one can achieve very low conductance values. For only five layers of black phosphorene (2.5 nm length) sandwiched between gold contacts, we calculate a thermal conductance of 4 MW m$^{-2}$ K$^{-1}$ for an ideal (defect-free) case. The value can be substantially smaller in practice due to imperfections. One can further decrease it by purposely introducing defects at the interfaces. As long as the defects do not block electrical transport and do not break the ballistic transport condition inside the barrier region, such an approach is an acceptable way of increasing the interfacial thermal resistance and, therefore, the efficiency. Other weakly bonded structures also demonstrate extremely low thermal conductance values. It was recently shown that interfacial thermal conductance between seven layers of $MoS_2$ and $c$-Si is smaller than 1 MW m$^{-2}$ K$^{-1}$ [13]. In another work, a graphene-$WSe_2$-graphene structure is proposed for thermionic power generation, and the thermal conductance was estimated to be around 0.5 MW m$^{-2}$ K$^{-1}$ [14]. Increasing the thermal resistance while maintaining a low electrical resistance remains the biggest challenge for solid-state thermionic devices.

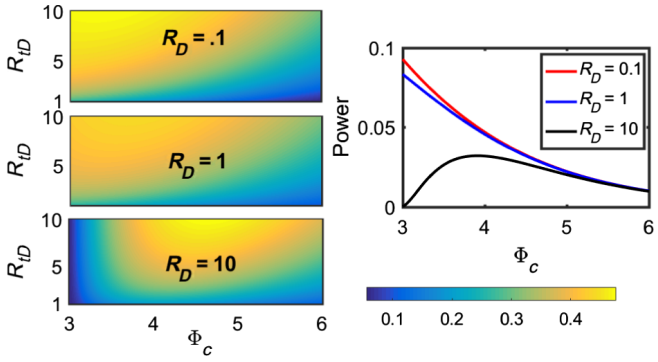


FIG. 2. Left: Efficiency at the optimum power calculated using Eq. (24) for $\theta = 1.5$ ($\eta_{\text{Carnot}} = 33\%$) and versus three main identified dimensionless parameters $\Phi_c$, $R_{tD}$, *and* $R_D$. Right: Optimum power (dimensionless) using Eq. (23) versus the cathode's barrier height for three different $R_D$ values.

Equations (23) and (24) show that there are only four independent parameters determining the efficiency: $R_{tD}$, $R_D$, $\Phi_c$, and $\theta$. This is similar to the case of thermoelectric materials. Here, $\Phi_c$, or more accurately, $\Phi_c + 2$, is the average energy carried per carrier and the equivalent of a dimensionless Seebeck coefficient. Similar to thermoelectric materials, the parameters are related. In some cases, they cannot be tuned independently, and in some other cases, the optimum value of one parameter depends on the other parameters. For example, as we increase the barrier height ($\Phi_c$), the average energy per carrier increases, resulting in enhanced efficiencies. At the same time, as the barrier height increases, the Richardson current decreases, lowering the optimum power. Also, at lower current values, larger thermal resistances are required to obtain reasonable efficiency values (as discussed before, $J_c R_{tD}$ is the relevant parameter).

Figure 2 shows the efficiency divided by the Carnot efficiency for $\theta = 1.5$ (or $\eta_{\text{Carnot}} = 33\%$) for three different electrical resistances and versus thermal resistance and barrier height. It also shows the optimum dimensionless power for the same electrical resistance values. As $R_D$ increases, the power drops as expected (note that the power is independent of the thermal resistance). $P_D$ (dimensionless power) of 0.01 is equal to power density of $p = 0.01(k_B T_a A_R T_a^2/e)$. At room temperatures, this value is $p = 3$ kW cm$^{-2}$. Therefore, we can judge that the power values reported in Fig. 2 are, in fact, very large, 100 times more than the reported values for vacuum-state thermionic generators. The reason is the substantially lower barrier heights. In terms of efficiency, as $R_D$ increases, the optimum value of $\Phi_c$ slightly shifts to larger values, but overall, it is somewhere between 3 and 5. So one can fix the value of $\Phi_c$ and try to optimize the values of the resistances. Assuming the structure is fixed and the contact layers (between cathode and barrier and between the barrier and

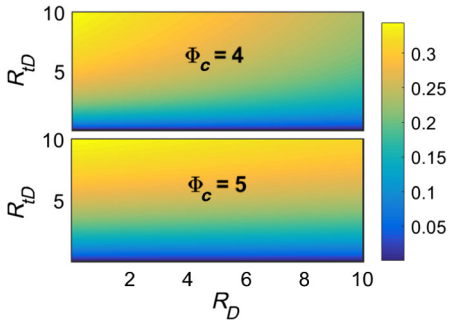


FIG. 3. Efficiency at the optimum power calculated using Eq. (23) for $\theta = 1.5$ and versus dimensionless thermal and electrical resistances. Here we fix the barrier height close to the optimum value identified from Fig. 3, which we fix the barrier height to be 4 in the upper plot and 5 in the lower plot.

anode) are optimized to have the largest possible interfacial thermal resistance and lowest possible interfacial electrical resistance, the only parameter to adjust is the thickness of the barrier. We can assume that both electrical and thermal resistances increase linearly with increasing the thickness. Figure 3 shows that for $\Phi_c = 5$, the efficiency is almost independent of the choice of $R_D$, and, therefore, we can increase the thickness to increase the thermal resistance and the efficiency. This insensitivity to thermal resistance can be explained as follows. For this barrier height, $J_c$ is 0.015, which means that even for $R_D = 10$, the value of $J_c R_D$ is 0.15, which is considered to be much smaller than 0.5 and satisfies the criterion of $2J_c R_D \ll 1$. The behavior is different for $\Phi_c = 4$. Here the efficiency slightly drops as $R_D$ increases (due to smaller $J_c$ values). As we increase the $R_{tD}$, $R_D$ also increases, and, therefore, the efficiency may or may not increase depending on the slope of $R_{tD}/R_D$.

Next, we show that it is also possible to find analytical solutions for optimum efficiency. The optimum current that results in the optimum efficiency can be estimated as

$$J_D = J_c y_0, \tag{25}$$

$$\beta k = \frac{(\Phi_c\theta + 2)}{(2 + \frac{1}{J_c R_{tD}})(\theta - 1)}, \tag{26}$$

$$y_0 = 1 - \frac{1 + \beta k}{LW(x_1)}, \tag{27}$$

$$x_1 = \theta^2(1 + \beta k)\exp\left\{J_c R_D\left[-2 + \beta k\left(-1 + \frac{1}{J_c R_D}\right)\right] + \Phi_c(\theta - 1)\right\}. \tag{28}$$

Plugging in this current, we find efficiency to be

$$\eta_{\text{opt}} = \frac{y_0 \ln(\frac{J_a}{J_0}) - J_c R_D y_0^2}{(2 + \frac{1}{J_c R_{tD}})(\theta - 1) + y_0(\Phi_c\theta + 2)}. \tag{29}$$

When we plot the results of Eq. (29) we do not see much difference between results of Eqs. (29) and (24), which means the results reported in Fig. 2 stay more or less the same if we try to optimize the efficiency instead of the power. Since the results are so similar, we do not report them here. If we look back at Fig. 1, we see that this similarity is expected since the optimum power and optimum efficiency occur at very close current values. The only exception is when the cathode work-function value is close to the anode one. In that case, optimum efficiency and optimum power can occur at distinct currents. Houston [15] numerically showed that at optimum conditions, the following relation roughly holds between the cathode and anode work function: $\Phi_c = \Phi_a$. For $\theta = 1.5$, which we use in our example, Houston criteria means the work function of the cathode is 1.5 times that of the anode. In this regime, our assumptions are correct.

Finally, we compare the performance of the thermionic power generators with thermoelectric modules. If we set $\theta = 1.5$ or $\eta_{\text{Carnot}} = 33\%$, the equivalent efficiency of an ideal thermoelectric modules for $ZT = 1, 2, 3$, $\eta_{\text{TE}}/\eta_{\text{carnot}}$ is equal to 0.19, 0.30, and 0.37 respectively. Figure 2 shows that using thermionic generators, and for the same $\theta$, efficiency values as high as $0.4\eta_{\text{carnot}}$ are achievable. In a large area of this graph, the efficiency values are higher than 0.19. For example, if we set the cold side temperature to 300 K and the hot side to 450 K, we can recover $\theta = 1.5$. For this temperature range, there are only a few thermoelectric materials available, and bismuth antimony telluride is the best candidate [16]. The peak $ZT$ value of $p$-type bismuth antimony telluride is 1.8 [17]. However, the average $ZT$ of $n$-type and $p$-type bismuth antimony telluride in this temperature range is much smaller and close to 1, which means with the known thermoelectric modules, the efficiency values higher than 20% of the Carnot efficiency are not achievable in this temperature range. But by using thermionic modules (Fig. 2), such efficiency values are easily achievable. At the same time, due to their smaller size, thermionic power generators own larger power density values, and, therefore, they could be potentially a better alternative to thermoelectric modules. One remaining question is if the set of parameters used in Figs. 2 and 3 is an achievable set or not. We note that for barrier height of 5, the results are independent of electrical resistance up to $R_D$ of 10 and even more. Therefore, we can simply ask if $R_{tD}$ of 5 and more is possible. If we again use the theoretical Richardson constant of 120 $\text{A cm}^{-2}\,\text{K}^{-2}$ and cold side temperature of 300 K, then $R_{tD}$ of 5 is equivalent to thermal conductance of 1.8 $\text{MW m}^{-2}\,\text{K}^{-1}$. As discussed before, it is challenging but not impossible to have such low conductance values at small scales. Note that the value of the conductance is higher for higher temperatures. For example, for the same $R_{tD}$ of 5, the equivalent conductance at 500 K is 5 $\text{MW m}^{-2}\,\text{K}^{-1}$. Also note that in practical devices, $A_R$ can significantly deviate from the theoretical

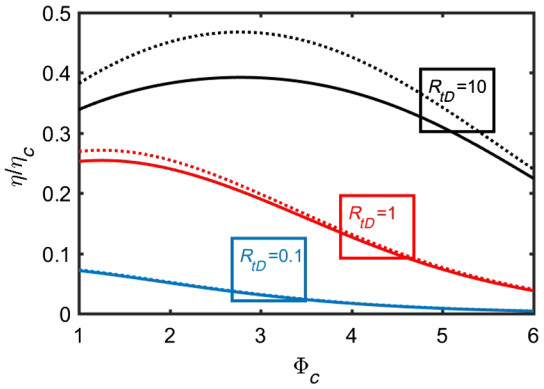


FIG. 4. Comparison of our results with those predicted by Mahan *et al.* in the limit of zero internal resistance and small temperature differences: $\theta = 1.05$ and $R_D = 0$. Solid lines result from using Eq. (24) and dashed lines are plotted using Eq. (24) of Ref. [1].

Richardson constant, and it will depend on the transmission function from the cathode to the anode significantly. Therefore, a clever design can have larger $A_R$ to further increase acceptable thermal conductance values.

Here we provide a discussion of the difference between our results and those obtained originally by Mahan *et al.* [2,18]. In their pioneering work, they assumed no internal resistance, small voltage, and temperature differences over *symmetric* barriers, allowing them to use Taylor expansions and to address the problem within the linear transport regime. Our focus is the alternative regime where tall barriers and large temperature differences are of interest. We also include the internal resistance which we believe can substantially lower the performance of the device. One question then is to what extent will our results tend to the work of Mahan *et al.* Since we do not assume a symmetric barrier, and instead, we assume the cathode work function to be larger than the anode work function, it is not trivial that we recover the results of Mahan *et al.* even in the linear regime. However, upon plotting the results in this limit, we find that our results are very similar to the results of Mahan *et al.* Figure 4 shows a comparison for small values of $\theta = 1.05$ and zero internal resistance. The difference between our results and theirs increases as thermal resistance increases, but as Fig. 4 shows, the differences are not large. Interestingly, we observe that even when larger $\theta$ values are used, our results are close to the predictions of Mahan *et al.* Therefore, as long as the internal electrical and thermal resistances are negligible, the formula of Mahan *et al.* can be used to estimate the performance of thermionic devices even at larger $\theta$ values. As we increase either $\theta$, $R_D$, or $R_t$, the optimum value of the barrier height tends to increase. The conclusion of Mahan *et al.* that the optimum barrier height is around $2k_BT$, therefore, is valid only in the linear regime. In the nonlinear regime and within reasonable values of thermal and electrical resistances, the optimum barrier height shifts to 3 to $5k_BT$. Finally, the reader should note that the conclusion of Mahan *et al.* that thermionic devices are not as good as thermoelectric devices, is valid only in the linear regime and if thermal resistance is dominated by the barrier lattice resistance. In the case where the thermal resistance of thermionic devices dominantly comes from the interfacial resistances, such a conclusion cannot be drawn, and thermionic convertors can be better than thermoelectric convertors.

## IV. CONCLUSION

In summary, we provide guidelines for the design of solid-state thermionic power generators. Although it is known that large thermal resistances and small electrical resistances are needed for these devices, here, we introduce quantitative measures to estimate the acceptable range of thermal and electrical resistances. If the internal electrical resistance is low so that $J_cR_D < 0.5$, and if the internal thermal resistance is large so that $J_cR_{tD} > 1$, then the performance is not affected, and there is no need to push the resistance values any further. We show that similar to the case of thermoelectric modules, there are four independent parameters determining the efficiency: $\Phi_c, R_D, R_{tD}$, and $\theta$. We discuss that these parameters are related. In some cases, they cannot be independently tuned, and in some other cases, their optimum value depends on the other parameters. We find the analytical expressions for the optimum load resistance as a function of the internal resistance which can be used when designing thermionic power generators for specific applications. When the internal electrical resistance is zero and for small values of thermal resistance, our results tend to those of Mahan *et al.*, even under large temperature differences. However, we find that the optimum barrier height in the nonlinear regime is larger than $2k_BT$ predicted by Mahan *et al.* in the linear regime. This optimum shifts to larger values for larger resistances. Finally, we demonstrate that by choosing the right parameters, thermionic generators can achieve efficiencies higher than the state-of-the-art thermoelectric modules.

## ACKNOWLEDGMENTS

The author acknowledges Joseph A. King, Jr., the Advanced Research Projects Agency-Energy (Arpa-e) for suggesting the problem and K. Esfarjani for his helpful feedback on the manuscript. This work is supported by the Air Force Young Investigator Grant No. FA9550-14-1-0316.

## APPENDIX: LAMBERT *W* FUNCTION

Equation (17) after neglecting the second-order term can be written as

$$\theta^2 \exp[(\theta-1)\Phi_c + 1 - 2J_cR_D] = \frac{J_c}{J_a}\exp\left(\frac{J_c}{J_a}\right). \quad \text{(A1)}$$

The solution of this equation is the Lambert $W$ function:

$$\frac{J_c}{J_a} = LW\{\theta^2 \exp[(\theta-1)\Phi_c + 1 - 2J_c R_D]\} = LW(x_0). \tag{A2}$$

For small temperature differences $\theta \sim 1$ and negligible internal resistances, values of $x_0$ are close to $e = 2.7$. The Lambert $W$ function of $e$ is equal to 1 [$LW(e) = 1$], and it decreases to values smaller than 1 as we decrease $x_0$. This means, $x_0$ values smaller than $e$ are not of interest, since for such values, the leak current ($J_a$) is larger than the cathode current ($J_c$). For large temperature differences and tall barriers, the values of $x_0$ can quickly increase. For example, $\theta = 2$, $\Phi_c = 10$, and neglecting electrical resistance gives $x_0 = 239 \times 497$. If needed, we can use simplified equations to estimate the $LW$ function. We find that using the following fits, one can accurately reproduce the $LW$ function. However, the final equation for efficiency does not simplify enough to justify the use of these fits:

$$LW(x) = \begin{cases} \ln(x) - \ln[\ln(x)] + 0.3, & 10 < x, \\ 0.58\ln(x) + 0.4, & 2.7 < x < 10. \end{cases} \tag{A3}$$


[1] G. D. Mahan, J. O. Sofo, and M. Bartkowiak, Multilayer thermionic refrigerator and generator, J. Appl. Phys. **83**, 4683 (1998).

[2] G. D. Mahan and L. M. Woods, Multilayer Thermionic Refrigeration, Phys. Rev. Lett. **80**, 4016 (1998).

[3] A. Shakouri, C. LaBounty, P. Abraham, J. Piprek, and J. E. Bowers, Enhanced thermionic emission cooling in high barrier superlattice heterostructures, Mater. Res. Soc. Symp. Proc. **545**, 449 (1999).

[4] A. Shakouri and J. E. Bowers, Heterostructure integrated thermionic coolers, Appl. Phys. Lett. **71**, 1234 (1997).

[5] V. C. Wilson, Conversion of heat to electricity by thermionic emission, J. Appl. Phys. **30**, 475 (1959).

[6] G. Hatsopoulos and J. Kaye, Analysis and experimental results of a diode configuration of a novel thermoelectron engine, Proc. IRE **46**, 1574 (1958).

[7] W. J. Bifano and R. M. Williams, Jr., NASA Report No. NASA-TN-D-4533, 1968.

[8] C.-C. Chen, Z. Li, L. Shi, and S. B. Cronin, Thermoelectric transport across graphene/hexagonal boron nitride/graphene heterostructures, Nano Res. **8**, 666 (2015).

[9] X. Wang, M. Zebarjadi, and K. Esfarjani, First principles calculations of solid-state thermionic transport in layered van der Waals heterostructures, Nanoscale **8**, 14695 (2016).

[10] S.-J. Liang, B. Liu, W. Hu, K. Zhou, and L. K. Ang, Thermionic energy conversion based on graphene van der Waals heterostructures, Sci. Rep. **7**, 46211 (2017).

[11] C. B. Vining and G. D. Mahan, The $B$ factor in multilayer thermionic refrigeration, J. Appl. Phys. **86**, 6852 (1999).

[12] H. Moss, Thermionic diodes as energy converters, J. Electron. Control **2**, 305 (1957).

[13] P. Yuan, C. Li, S. Xu, J. Liu, and X. Wang, Interfacial thermal conductance between few to tens of layered-MoS 2 and $c$-Si: Effect of MoS 2 thickness, Acta Mater. **122**, 152 (2017).

[14] M. Massicotte, P. Schmidt, F. Vialla, K. Watanabe, T. Taniguchi, K. J. Tielrooij, and F. H. L. Koppens, Photo-thermionic effect in vertical graphene heterostructures, Nat. Commun. **7**, 12174 (2016).

[15] J. M. Houston, Theoretical efficiency of the thermionic energy converter, J. Appl. Phys. **30**, 481 (1959).

[16] A. Mehdizadeh Dehkordi, M. Zebarjadi, J. He, and T. M. Tritt, Thermoelectric power factor: Enhancement mechanisms and strategies for higher performance thermoelectric materials, Mater. Sci. Eng. R **97**, 1 (2015).

[17] S. Kim, K. H. Lee, H. A. Mun, H. S. Kim, S. W. Hwang, J. W. Roh, D. J. Yang, W. Shin, X. S. Li, Y. H. Lee, and G. J. Snyder, Dense dislocation arrays embedded in grain boundaries for high-performance bulk thermoelectrics, Science **348**, 109 (2015).

[18] G. D. Mahan and J. O. Sofo, The best thermoelectric, Proc. Natl. Acad. Sci. U.S.A. **93**, 7436 (1996).